remote sensing

MDPI

Article

Monitoring Coastal Evolution and Geomorphological Processes Using Time-Series Remote Sensing and Geospatial Analysis: Application Between Cape Serrat and Kef Abbed, Northern Tunisia

Zeineb Kassouk [1,*], Emna Ayari [1], Benoit Deffontaines [2] and Mohamed Ouaja [3]

[1] National Agronomic Institute of Tunisia, Carthage University, LR 17AGR01 (Lr GREEN-TEAM), 43 Avenue Charles Nicolle, Tunis 1082, Tunisia; ayari.emna.inat@gmail.com
[2] Laboratoire Géomatériaux et Environnement, Université Gustave Eiffel, 77420 Champs-sur-Marne, France; benoit.deffontaines@univ-eiffel.fr
[3] Department of Geology, Faculty of Science, Gabes University, Gabes 6072, Tunisia; mohamedouaja@yahoo.fr
* Correspondence: zeineb.kassouk@inat.ucar.tn; Tel.: +216-95458724

Abstract: The monitoring of coastal evolution (coastline and associated geomorphological features) caused by episodic and persistent processes associated with climatic and anthropic activities is required for coastal management decisions. The availability of open access, remotely sensed data with increasing spatial, temporal, and spectral resolutions, is promising in this context. The coastline of Northern Tunisia is currently showing geomorphic process, such as increasing erosion associated with lateral sedimentation. This study aims to investigate the potential of time-series optical data, namely Landsat (from 1985–2019) and Google Earth® satellite imagery (from 2007 to 2023), to analyze shoreline changes and morphosedimentary and geomorphological processes between Cape Serrat and Kef Abbed, Northern Tunisia. The Digital Shoreline Analysis System (DSAS) was used to quantify the multitemporal rates of shoreline using two metrics: the net shoreline movement (NSM) and the end-point rate (EPR). Erosion was observed around the tombolo and near river mouths, exacerbated by the presence of surrounding dams, where the NSM is up to −8.31 m/year. Despite a total NSM of −15 m, seasonal dynamics revealed a maximum erosion in winter (71% negative NSM) and accretion in spring (57% positive NSM). The effects of currents, winds, and dams on dune dynamics were studied using historical images of Google Earth®. In the period from 1994 to 2023, the area is marked by dune face retreat and removal in more than 40% of the site, showing the increasing erosion. At finer spatial resolution and according to the synergy of field observations and photointerpretation, four key geomorphic processes shaping the coastline were identified: wave/tide action, wind transport, pedogenesis, and deposition. Given the frequent changes in coastal areas, this method facilitates the maintenance and updating of coastline databases, which are essential for analyzing the impacts of the sea level rise in the southern Mediterranean region. Furthermore, the developed approach could be implemented with a range of forecast scenarios to simulate the impacts of a higher future sea-level enhanced climate change.

Keywords: coastal change; time-series satellite data; geomorphological processes; DSAS; dune evolution

Citation: Kassouk, Z.; Ayari, E.; Deffontaines, B.; Ouaja, M. Monitoring Coastal Evolution and Geomorphological Processes Using Time-Series Remote Sensing and Geospatial Analysis: Application Between Cape Serrat and Kef Abbed, Northern Tunisia. *Remote Sens.* **2024**, *16*, 3895. https://doi.org/10.3390/rs16203895

Academic Editors: José Juan de Sanjosé Blasco, Germán Flor-Blanco and Ramón Blanco Chao

Received: 31 July 2024
Revised: 16 August 2024
Accepted: 17 August 2024
Published: 19 October 2024

1. Introduction

Coastal areas have paramount importance for the high productivity of the ecosystem, urban concentration, and the exploitation of natural resources. The coastline, identified as the boundary between the land and the sea, occupies more than 10% of the earth's surface, and about 42% of the world's population lives within 100 km from the coastline [1]. Under the climate change impact, the rising sea levels can create pressures on the physical coastline, as well as on coastal ecosystems [2].

Consequently, the coastal region is highly vulnerable and heavily exposed to various natural disasters, such as storm surges, sea level rise, tidal floods, erosion, the shifting of the shoreline [3–7]. Additionally, the intensification of human activities, such as artificial berm-building and dams and the increase population density on coastal zones lead to frequent coastline changes [8,9].

Many approaches for detecting changes in coastlines over time developed based on ground observations and surveys using GPS [10–12] or other surveying equipment to directly measure and map the coastline change. Despite the accurate information provided by in situ measurements, they are insufficient for monitoring spatiotemporal coastline dynamics. Therefore, several efforts have been devoted to investigating remote sensing technologies to monitor the aforementioned coastal dynamics during several periods and erratic geomorphological changes (e.g., erosion patterns, sedimentations, and landscape changes) [6,13–16].

Many researchers focused on monitoring changes in coastline and other coastal physical features using satellite and unmanned aerial vehicle (UAV) data [16–24], such as LiDAR [10,12,24–28]. Those technological approaches enable the effective tracking of environmental transformations over time, providing critical insights into coastal dynamics, habitat alterations, and the broader impacts of climate change [29].

Owing to the availability of open access satellite data, several approaches quantified shorelines movements and highlighted the dynamic coastal evolution based on optical [27] or radar images [1,8,16,24,27,30,31] or the synergy between them [28,32].

Spectral information derived from airborne and satellite data is widely used to differentiate between water, bare soil, and vegetated areas by applying several approaches [10,14,22,25,27,28,33–35]: the segmentation-based method, classification-based methods, and hybrid methods. The segmentation is based on feature extraction using either thresholding or morphological filters to detect edges [17,19,24,33,34]. Several studies proposed hybrid approaches mixing between the classification and/or segmentations and photointerpretation or probabilistic models [35]. These aforementioned methods can be coupled with machine learning algorithms, such as the neural network algorithm and data mining techniques [6,9,12,36,37].

Several researchers used derived spectral information such as principal component analysis (PCA) [26,27] or spectral indices derived from satellite images (band ratio, band difference, normalized indices). The Normalized Difference Vegetation Index (NDVI) [19,20] and the Normalized Difference Water Index (NDWI) [18] are applied to delineate shoreline geometry, which is defined as the wet–dry boundary, highlighting the upper limit of coastal wetting caused by the last high [38]. Based on these various approaches, several previous works proposed a coastline delineation product at global and regional scales [8,10,16,18,22,27,36,39]. Other methods focus on the change detection of ecological coastal unit identified by using a combined geospatial approach field observation and existing data [40]. Although previous works proved the performance of these algorithms in extracting coastlines, they mentioned obvious difficulties in dealing with coastal dune dynamics [19,26,37].

The aims of this study, carried out in the northern of Tunisia, are the following:

- Understand the trend of shoreline changes over the period of 1985–2023 using multisensory remote sensing data and field observations.
- Identify the geomorphological processes and rates of shoreline changes, including both erosion and accretion patterns.
- Explore how the remote sensing and geospatial analysis techniques employed in this study can be extended to other coastal regions in Tunisia or the broader Mediterranean basin to develop a comprehensive understanding of regional coastal dynamics.

The proposed approach, which involves the use of historical remotely sensed data, baselines, transects, and change detection, is expected to provide valuable insights into the coastal processes and support the development of effective coastal management policies in the region.

2. Materials and Methods

2.1. The Study Area

2.1.1. The Study Area Location

The study area is situated along the northern Tunisian coast, between Cape Serrat and Ragoubet el Golea rocky points (Figure 1). The coastline stretches over 20 km and includes a variety of morphological features, including a sandy coastal area, as well as recent dunes (Holocene), alluvial features, and predominantly sand dunes in the west. Tidal currents and wave action are reduced in the area due to low tide [38]. Plant communities range from pioneer vegetation near the shoreline to Mediterranean shrubs on the landward fixed dunes.

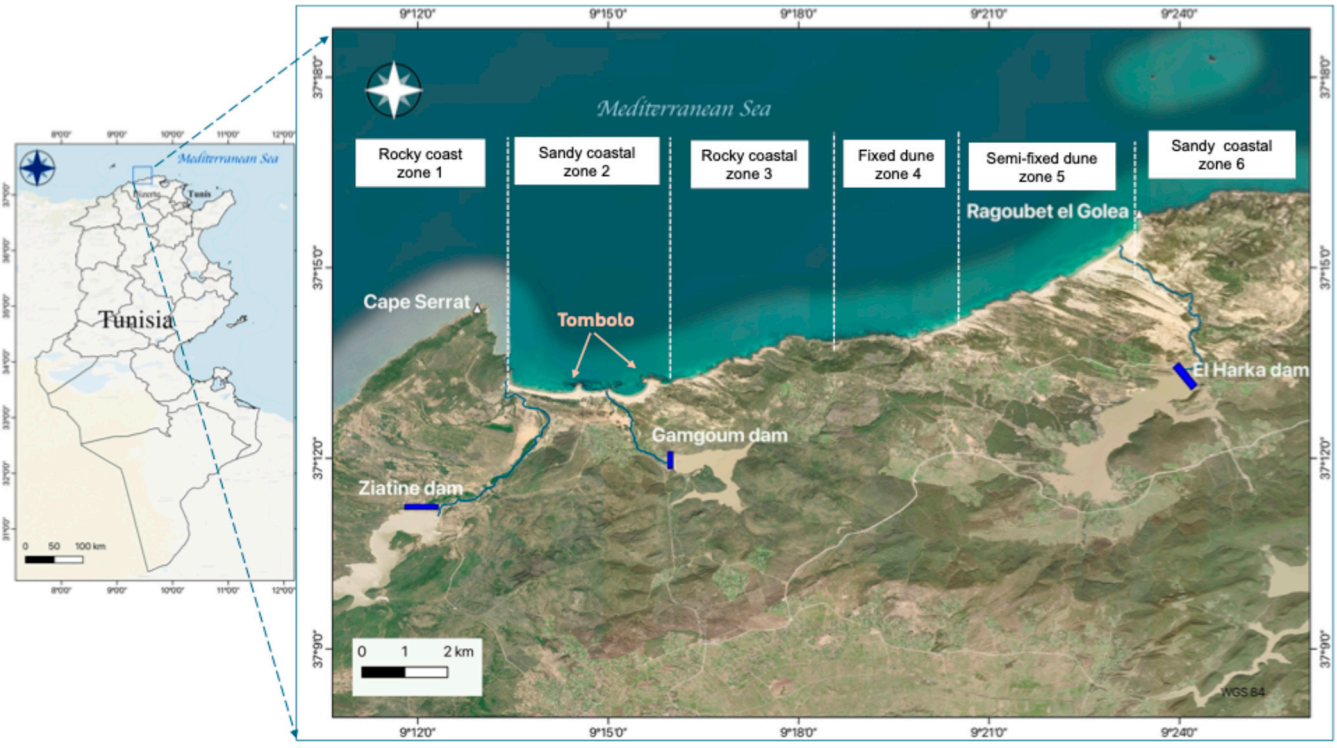

Figure 1. Location of the studied northern Tunisian coastal area (southern Mediterranean seashore) between Cape Serrat and Ragoubet El Golea, showing (blue rectangle) the three main dams and rivers, including Ziatine, Gamgoum, and El Harka. The study area was divided into six zones, according to their morphologies: Three zones are characterized by rocky coasts, a sandy coastal area with a tombolo, and fixed and (semi-)fixed dune zones. The background is the MapTiler Satellite map.

Depending on the sensitivity of the coastal zone, the area has been segmented into six distinct morphological sub-zones, as illustrated in Figure 1: three rocky coastal zones (zones 1, 3, and 6), a sandy coastal area (zone 2), including the Gamgoum River mouth and a tombolo (a sand and gravel bar connecting an island), as well as two zones of sandy coastal areas with developed dunes (fixed dunes in zone 4 and a semi-fixed dune in zone 5).

Over the past 40 years, the coastal ecosystem has faced a consistent processes of coastal erosion and the effects of three dams on the main rivers (Gamgoum, Ziatine in 2010, and El Harka in 2016) [3].

2.1.2. Wind and Hydrodynamic Characteristics

The study area is characterized by a subhumid climate with an annual precipitation average between 600 and 1000 mm. It is under the influence of winds predominantly from the west (west and west–northwest) with a maximum speed of 35 km/h. The wind-induced current velocities in the area range from 0.2 to 0.5 m/s. Significant swells were generated

with an amplitude ranging from 5 to 6 m. The dominant current directions, on average, are from east to south and west to north. The highest wave amplitudes occur in the early fall/winter, while the lowest wave amplitudes are observed in the summer. The offshore wave has a maximum amplitude of at least 2 m, and this occurs for the two dominant near-shore wave directions: north–west and west. The tidal range is relatively small, not exceeding 0.7 m [2,41,42].

2.2. Data and Methods

Remote Sensing Data

To reliably assess the seasonal and long-term evolution of the coastline, this study used the long temporal series Landsat data, over the period from 1985 to 2019. Landsat 5 Thematic Mapper (TM) was utilized from 1985 to 1998, followed by Landsat 7 Enhanced Thematic Mapper Plus (ETM+) from 1999 to 2013, and Landsat 8 Operational Land Imager (OLI) from 2013 to 2019.

Surface reflectance data Level 2 (L2) were downloaded using the Earth Engine platform (Table 1 and Supplementary Materials). Although the Landsat archive included provides continuous images, frequent cloud cover leads to significant temporal gaps in the data during specific periods (frequently in winter). To meet this study's objectives, we considered only cloud-free images.

Table 1. Characteristics of Landsat data used for seasonal and annual evolution of the coastline.

Landsat Sensor	Used Bands	Pixel Size	Seasonal Evolution				
			Winter	Spring	Summer	Fall	Considered Period
Landsat 5 L5 TM	1 to 5 and 7	30 m	5	11	15	6	From 1985 to 1998
Landsat 7 L7 ETM+	2, 3, 5	30 m	4	7	8	7	From 1999 to 2013
Landsat 8 L8 OLI	2 to 7	30 m	3	4	7	3	From 2014 to 2019

Landsat 7 ETM+ data acquired after May 2003 contained more than 22% of unscanned gap pixels, caused by the failure of the Scan Line Corrector (SLC), severely limiting their utility. To fill these gaps, the data were corrected using the SLC-off gap-filled products and the gap-fill algorithm methodology developed in Envi® [43]. For annual evolution, the image acquisition dates were as follows: (i) 19 November 1999 (Landsat 5), (ii) 20 November 2019 (Landsat 7), and (iii) 19 November 2021 (Landsat 8).

To analyze the coastline and its ecosystem dynamics, including dunes' changes, we used a high-resolution imagery offered by the Google Earth data. Owing to the launch of this platform in 2005, global collection of true colored images is available, cost-free and ready to use as a visualization tool [34,36,44,45]. The wide use of Google Earth images in geomorphological studies is attributable to its facility [46,47].

In the present study, changes in the dune system were observed and documented over the period from 2007 to 2023 using the ancillary Google Earth® achieve. The images were collected for the years 2007, 2010, 2012, 2014, 2016, 2019, and 2023, selected for their high spatial resolution and minimal cloud cover to ensure clear visibility of ground features.

2.3. Methodology

2.3.1. Coastal Area Change Detection Based on Coastline Monitoring

Figure 2 displays the flowchart outlining the steps for extracting the shoreline (coastline) and analyzing changes over time.

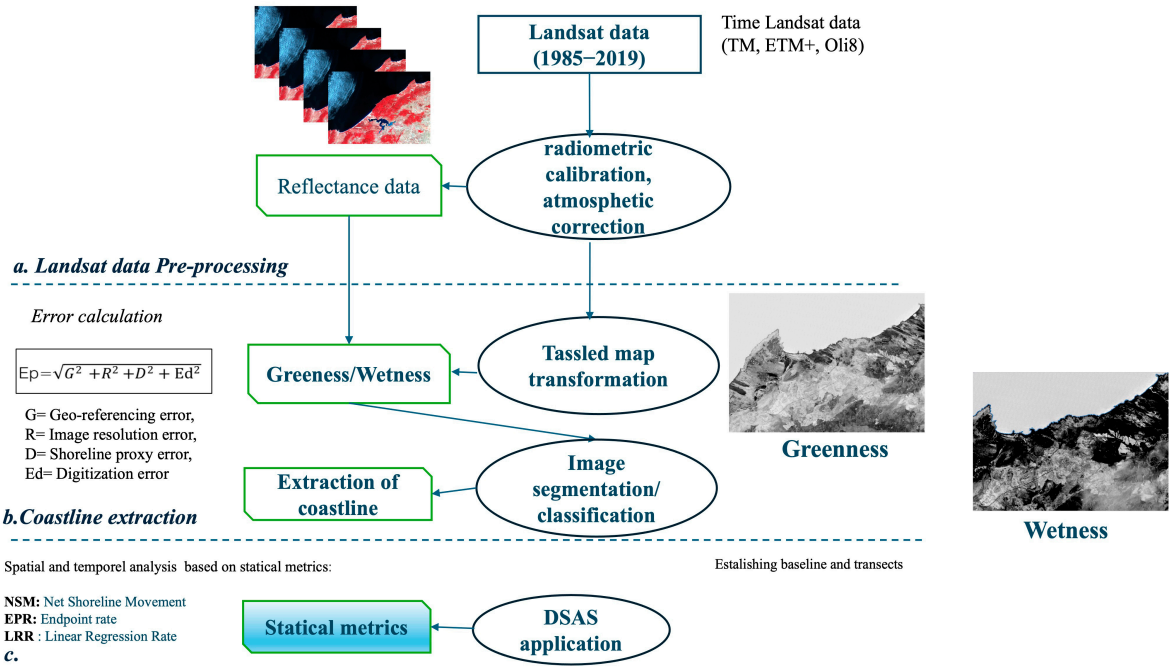

Figure 2. Flowchart related to Landsat data analysis for the years 1985–2019. It involves the following: (**a**) the pre-processes steps: radiometric calibration, geometric, and atmospheric corrections; (**b**) the multi-time coastline extraction based on the Tasseled map transformation (greenness/wetness data extraction); and (**c**) coastline evolution.

Coastline Extraction

To extract the coastlines from the Landsat time series, the Tasseled Cap Transformation (TCT) principal component analysis was applied [1,48]. This technique compresses the spectral information of the Landsat time-series data into a few key components. The most used components are brightness (related to soil), greenness (linked to vegetation), and wetness (describing the interrelationship between soil and canopy moisture) [1]. For the Tasseled Cap analysis, bands 1 to 5 and band 7 (Landsat 5 TM and Landsat 57 ETM+), as well as bands 2 to 7 (Landsat 8 OLI) were used (Table 1). By creating a sufficiently large database that can capture intra-annual (within-year) oscillations, this study aims to detect the overall trend in the seasonal and long-term coastline change.

As water bodies are characterized by high wetness values and low greenness, they can be differentiated from other image objects (such as vegetation, buildings, and bare soil) using threshold conditions. Specifically, the criteria used were wetness values > greenness values and wetness values < K, where K is an empirical constant of the greenness component, usually equal to 750 [48]. The resulting image was then segmented and classified to separate water bodies from the other image objects.

A first coastline shape was obtained by converting the sea-water body data into a vector format. These data contained some shorter line segments, primarily due to the removal of small water areas (less than 200 m^2). Furthermore, the inconsistent water content in the shallow regions made it challenging to accurately represent the water information, leading to interruptions in the detected coastline. The initial coastline information was manually refined by addressing the issues of short-line segments and discontinuous coastlines, using a combination of length-based filtering and geometric connectivity analysis to improve the representation of the coastline. The verification of coastline positions is conducted by comparing the extracted coastlines with high-resolution imagery from Google Earth® when available, as well as with ground truth data collected in 2019. Incoherent features were manually corrected.

Coastline Change Detection

To analyze historical coastal changes based on the shoreline digitized from time-series remote sensing images, the Digital Shoreline Analysis System (DSAS) algorithm implemented in ArcGIS® was used [49]. DSAS approach comprises three steps: the identification of a baseline, the identification of transects across the baseline, and the statical computing of change [22,37,49,50].

For each data acquisition, the baseline was first identified based on the dominant direction and parallel to the global shoreline orientation. Then, a buffer with a 200 m distance for each baseline was created. Then, transects perpendicular to the reference baseline and spaced 50 m apart were generated, and the distances between each coastline and the baseline were measured along each transect. The generated data were organized into the shoreline attributes table including year, ID, shape, and uncertainty.

The last step is quantifying the evolution rates of shoreline from 1985 to 2019 using statistical metrics produced by DSAS and based on historical shoreline database. Three statistical metrics were calculated with a confidence interval of 95.5%:

- The net shoreline movement (NSM) characterizing the distance (m) between the oldest and the youngest shorelines for each transect, indicating the total movement between the two shoreline positions.
- The end-point rate (EPR) is a measure of the rate of shoreline change. It is calculated as the ratio of the distance of shoreline movement to the time elapsed between the oldest and the most recent shoreline measurements. The EPR indicates the yearly rate of shoreline shifting, with a positive value representing a shifting towards the sea and a negative value representing a shifting towards the land.
- Linear Regression Rate (LRR), which is calculated using the least squares regression line from all shoreline positions along each transect.

For long-term analysis EPR was used, whereas for short-term analysis, LPR was applied to reduce errors [50].

The accuracy of results was calculated based on the residual error derived from the shoreline extraction (georeferencing image and normalization, image resolution, shoreline identification), the distance between transects, and the smoothing distance.

Landsat images from 1985, 1995, and 2015 and 2019 were used to determine differences in the shoreline course in subsequent years and to determine the extent of shifts/changes of the coastline in each period. Afterwards, the LRR, EPR, and NSM were measured along 50 m spaced transects for each Landsat image.

2.3.2. Dune System Mapping

Google Earth® satellite images (from 2007 to 2023) were carefully examined through on-screen digitization and visual interpretation. The dune system was delineated for each year, focusing on the spatial distribution, density, and types of vegetation present. The obtained maps characterizing the dune system over time were compared and analyzed to identify trends and changes in landscape over time.

Potential drivers of the observed changes, such as variations in environmental conditions or land management practices (e.g., the effects of dams), were considered and discussed based on the available information. Where possible, the interpreted results were validated based on field observations to ensure the reliability and accuracy of the photo interpretation.

3. Results

3.1. Main Coastline Changes

The high rate of erosion between the years of the period from 1985 to 2019 happened in many regions, especially near river mouths, with a minimum EPR value of −2.27 m/year (Figure 3).

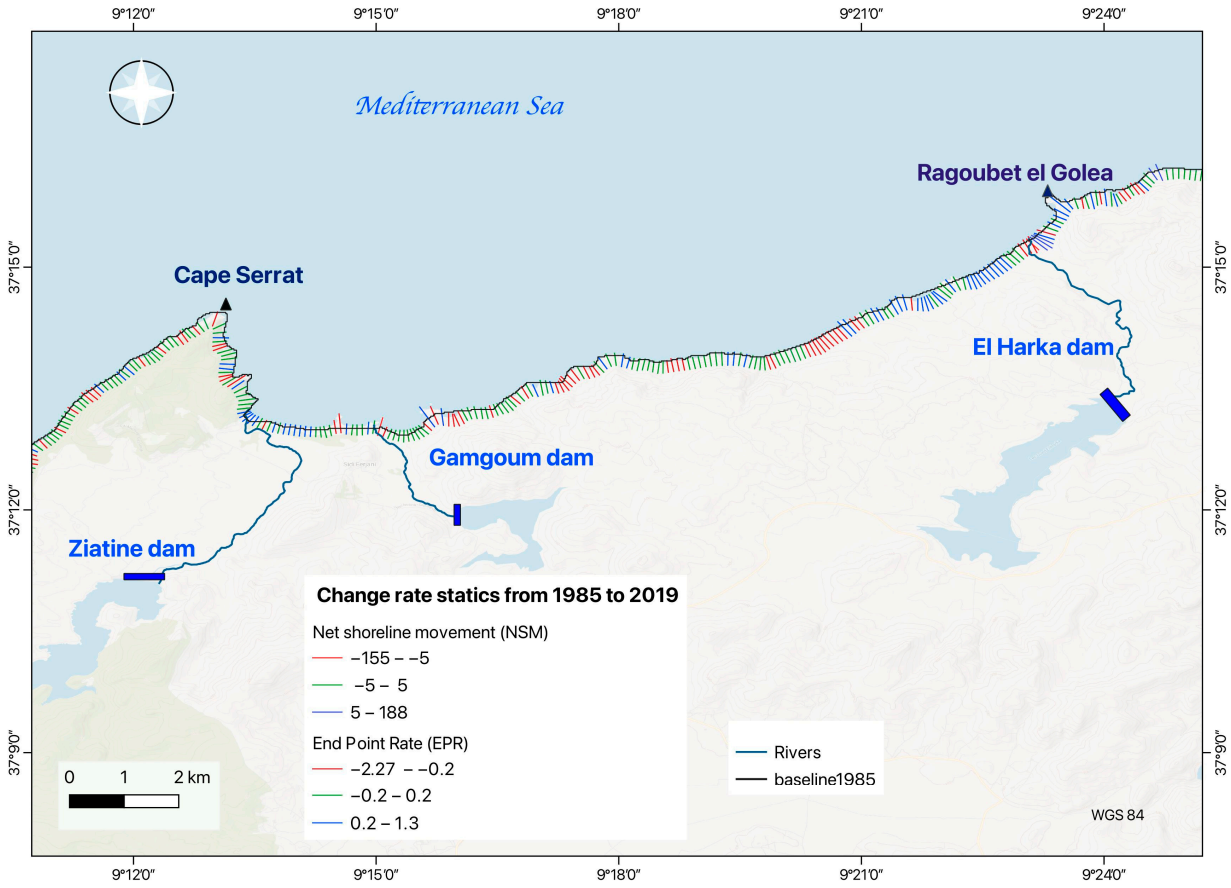

Figure 3. Net shoreline movement (NSM) in the period from 1985 to 2019 between Cape Serrat and Ragoubet el Golea points. Shoreline retreat is indicated by red lines, while green lines represent relatively unchanged areas. Shoreline advance is indicated by blue lines. The background is the MapTiler Topo map.

Negative NSM values (52% of the total observed data) point to erosion, while positive values point to accretion (48% of the total observed data). Maximum erosion (−100 m) is observed near the tombolo, with an average annual erosion of −2 m/year. Accretion is greatest in the area, with an annual rate of 1.3 m/year near the river mouth.

Figure 4 of the DSAS results for the tombolo area indicates the most significant loss of shoreline in the region, with the highest EPR (−2.27/year) and NSM (–155 m) values over the study period (from 1985 to 2019).

3.2. Seasonal Evolution of the Coastal Area

The seasonal sedimentary balance of shoreline movement (Figure 5a,b) highlights the maximum erosion in winter and maximum accumulation in spring. Effectively, during winter, winds move toward the low-pressure from the Mediterranean to the land causing the winter storm season. Negative NSM values indicate shoreline erosion or dune retreat and removal, suggesting that the shoreline moved away from a predefined baseline, especially during fall (58%) and winter (71%). The mean NSM values in this period are around −58 m and 48 m, respectively. The spring and summer NSM values are relatively high, at 31 m and 37 m.

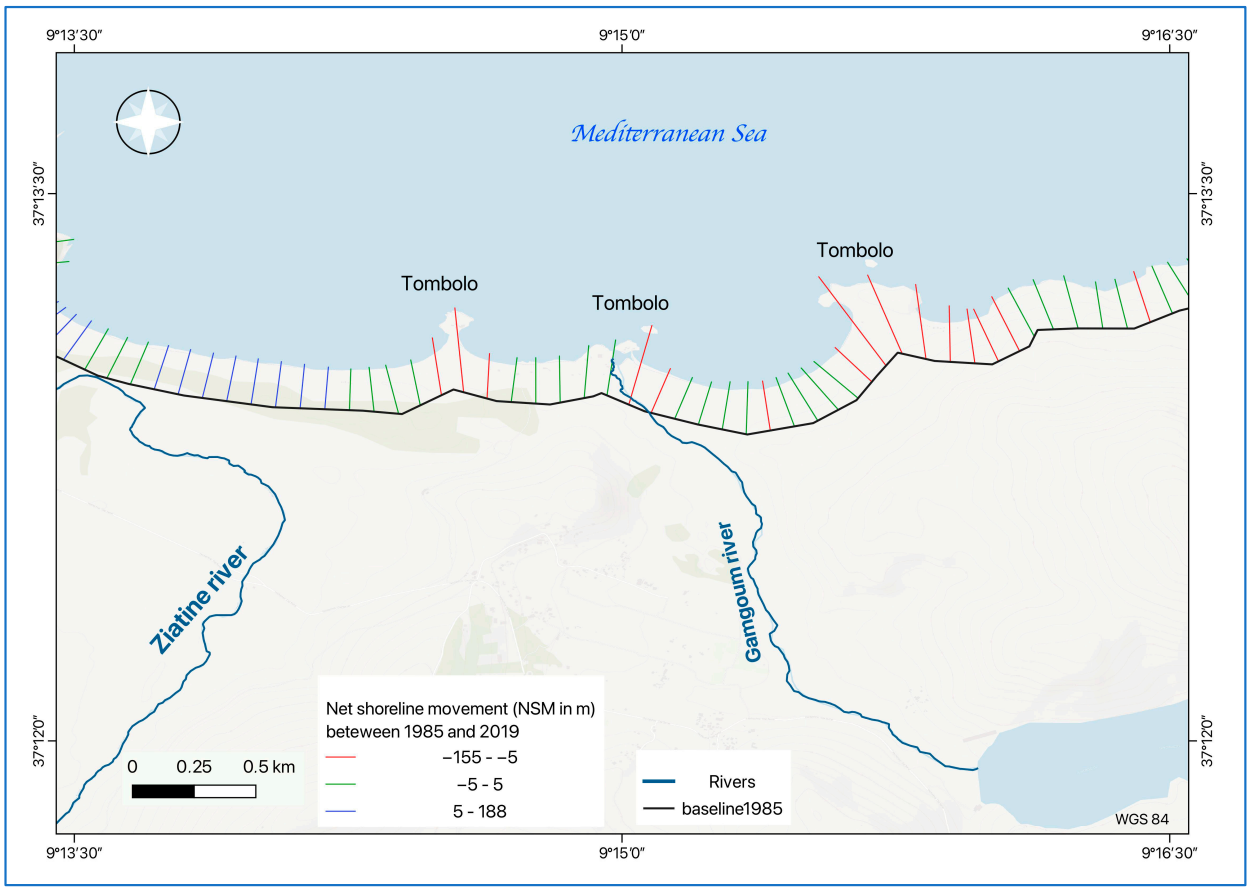

Figure 4. Erosion forms are mainly identified around the tombolo areas, indicated by red lines.

3.3. Coastal Dune and Vegetation Systems

To explore the different natural process and coastal features implicated into the erosion/accretion dynamics over the coast, we use finer high-resolution images, compared to the 30 m Landsat images, which furnish supplementary details. The photointerpretation of GoogleEarth® images highlights the coastal dune behavior and dynamic, which are mainly impacted by sand transport.

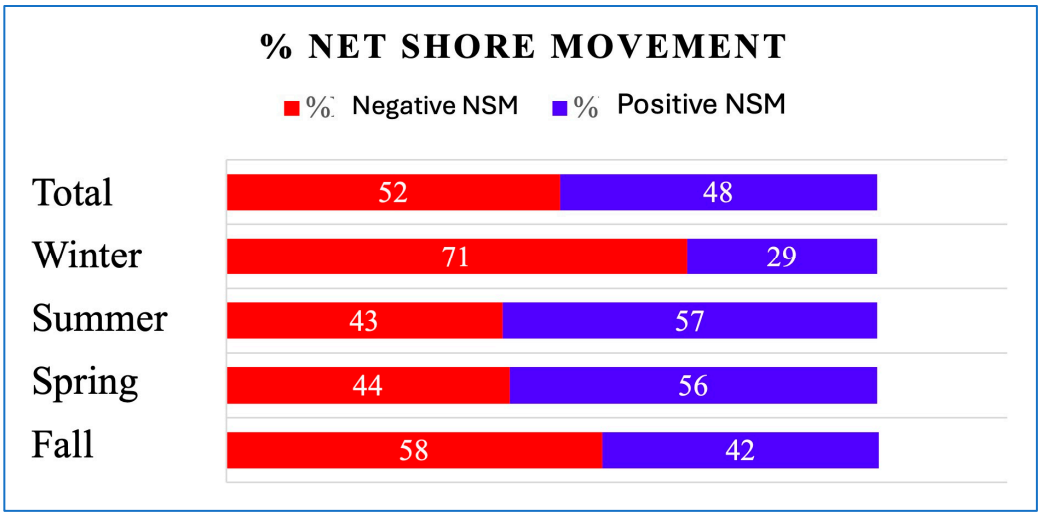

(**a**)

Figure 5. *Cont.*

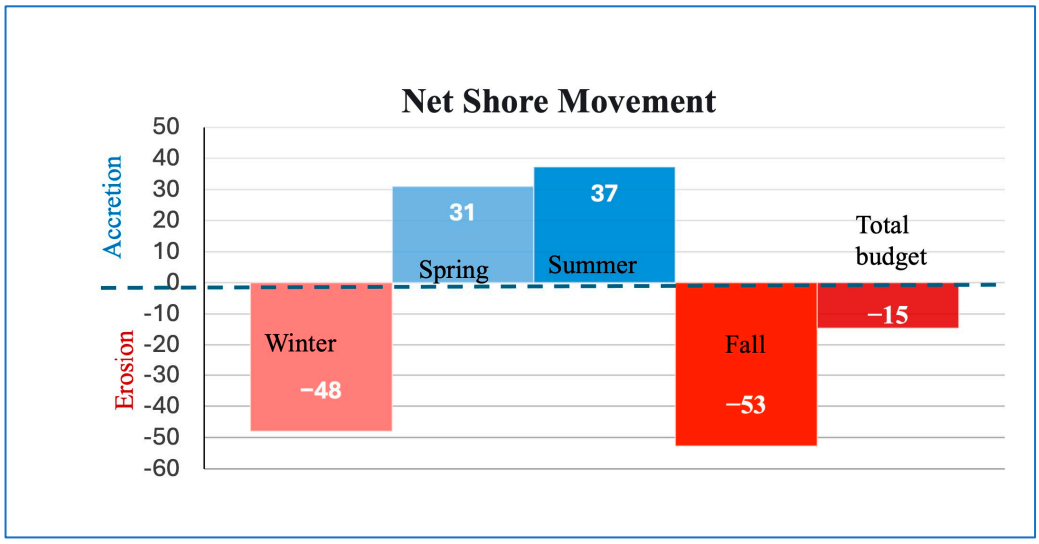

(**b**)

Figure 5. (**a**) Seasonal sedimentary balance of shoreline movement based on near-shore movement values (the distance between the oldest and youngest shorelines), net shoreline movement and (**b**) seasonal NSM variation showing the balance between erosion (blue color) and accretion (red color) and the total NSM value.

Figure 6 illustrates sandy coastal zone 2 (referenced in Figure 1), highlighting three distinct stages of dunes: high sand dune (L1), incipient dune (Level 2 or L2), and foredune (frontal, LN), which is heavily vegetated. The dense vegetation on the foredune helps stabilize the sand, reduces erosion, and contributes organic matter to the soil. It also plays a crucial role in the pedogenesis process, as it contributes to soil formation and stabilization, supporting diverse ecosystems in the coastal environment.

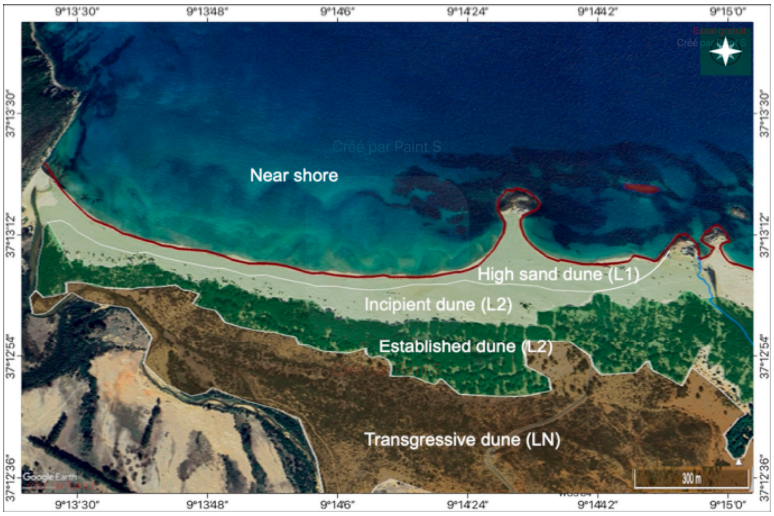

Figure 6. Spatial distribution of dunes as examples of different stages, from stable and vegetated dunes to system instability and the development of a mobile transgressive dune system. High sand dune (Level 1 or L1); incipient dune, L2, and foredune (LN) (background map is a GoogleEarth® image of 2019).

Increased erosion near the tombolo (Figure 7) and changes in wind patterns caused the disappearance of incipient dunes and the alteration the larger-scale dune morphology and dynamics. As the dunes are associated with the vegetation, the vegetation pattern

in lowlands between active sand dunes was delineated using the photointerpretation of GoogleEarth® images collected in 2007, 2010, 2012, 2014, 2016, and 2019.

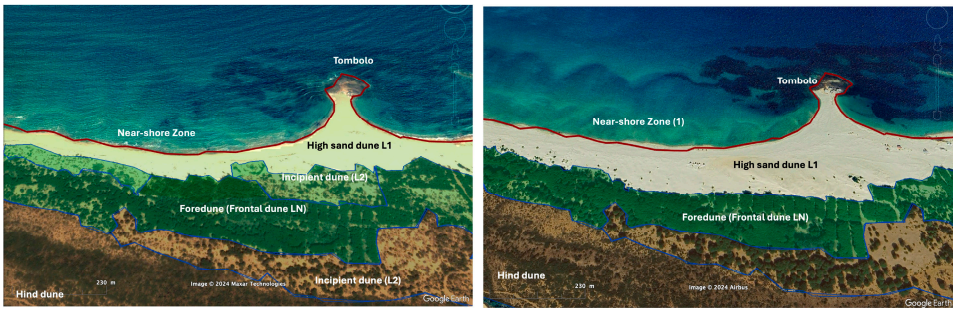

Figure 7. The disappearance of the incipient dune between 1994 and 2018, based on two satellite GoogleEarth® views. The phenomena highlight the important erosion process around the tombolo.

It highlights the costal geomorphology forms in 1994, regrouping the area close to the water affected by wave action (near-shore zone), the largest or most prominent dune in the system (high sand dune (L1)), the early stage of vegetated dune formation (incipient dune (L2)), and the established dunes at the front of the dune system (foredune (frontal dune LN)). Moreover, the 2019 GoogleEarth® view highlights the destruction of the incipient dune.

3.4. Geomorphological Process near Tombolo

Multidate Googleearth® imagery acquired from 2007 to 2023 (Figure 8) highlights the erosion near the tombolo area in zone 2 (referenced in Figure 1). In 2007, 2012, 2014, and 2016, the area was marked by the appearance of escarpments and the disappearance of comet tails, the deposition of sand and dune generation in the period from 2014 to 2023 near the tombolo, and the changes in sand forms and direction in 2019.

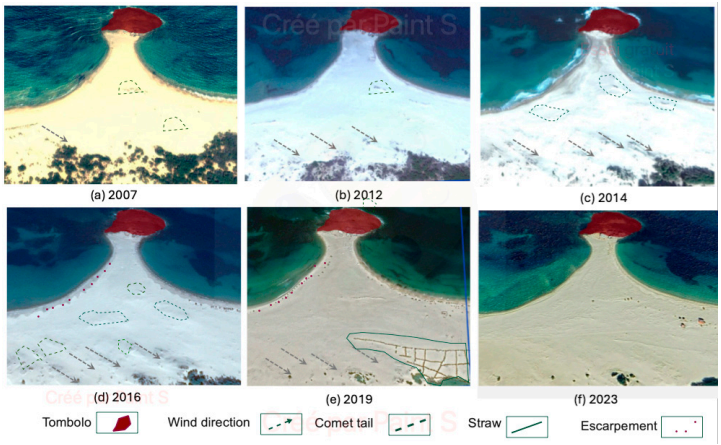

Figure 8. Example of wind action on the dunes based on GoogleEarth® time-series imagery (a view of zone 2 (Figure 1)). Green arrows highlight the perpendicular direction of the wind reactivation by a secondary wind from the north–east (NE) of the old dunes under the dominant north–west (NW) wind.

The escarpment suggests a shift in the prevailing wind direction from northwest (in 2014) to northeast (in 2016) (Figure 8). The dune stabilization straw structure built in 2019 (Figure 8e) was removed in 2023 (Figure 8f). These changes have implications for the overall coastal dynamics and the adaptation of the local forest line to the new environmental conditions of sand deposit resulted from erosion.

4. Discussion

4.1. Geomorphic Process in the Coastal Areas

The dynamic nature of coastal land identified by this study for the period from 1985 to 2019 shows an erosion trend, with 52% negative NSM. This behavior might be the result of natural causes (such as variability in sediment supply to the littoral zone, storm waves, long shore sediment transport) and anthropogenic causes (such as the dam construction), which induce the interruption of material in transport and reduce sediment supplies to the littoral zone.

The dune system in the study area (Figure 9) highlights the importance of the interplay between physical processes (wind, sand transport) and biological processes (vegetation establishment and soil development). This may be explained mainly by four geomorphic processes in the study area: (1) erosion and deposition processes caused by the movement of waves along the shoreline (in the near-shore zone); (2) strong wind erosion and transportation, creating features such as sand dunes and wind-carved rock formations; (3) pedogenesis, which leads to the stabilization and fixation of dunes through the growth of vegetation. This process is reflected in the color of the sand, mainly in the transgressive dune shown in Figure 9. (4) Deposition processes: note that the tide effect is not considerable in the study area because tide levels are less than 0.7 m.

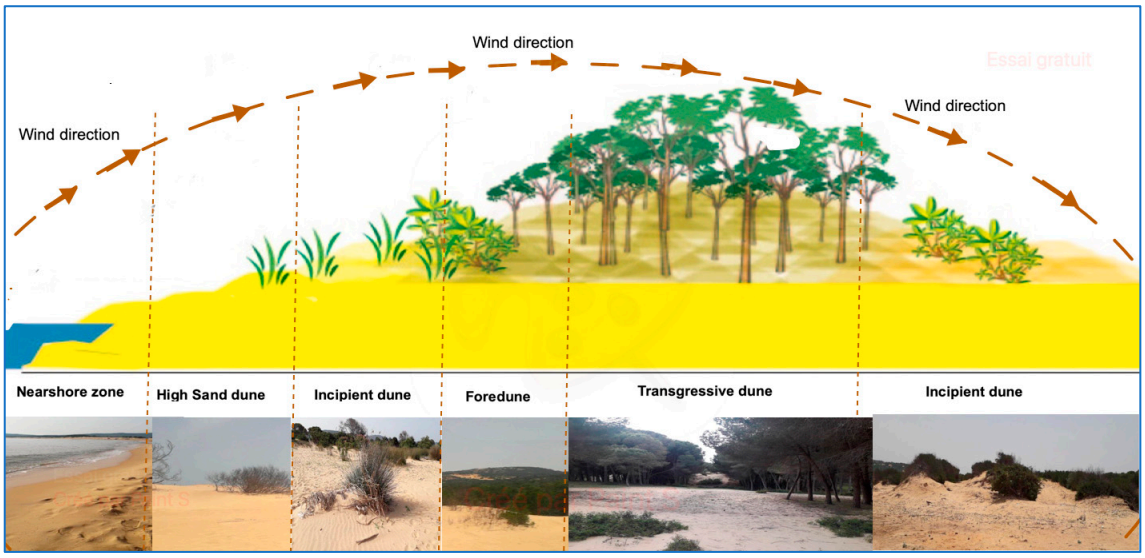

Figure 9. An example of dune zonation in the study area in relation to wind direction. Five categories of dunes were identified, including near-shore zones, high sand dunes, incipient dunes, foredunes, and transgressive dunes.

Vegetation in the dune landscape (such as dune grasses, shrubs, and trees) helps to stabilize the dunes and prevent sand from being carried away by the wind. It acts as a "wind barrier", providing stability and protection against wind erosion.

4.1.1. Effect of Current and Wind in Dunes near River Mouths

Two dune categories are observed according to their shape and size: large dunes with a gentle slope (less than 3%) caused by the interaction of multiple coastal currents on the windward side (NE-SW) (Figure 10a); short and steeper dune under the influence of a single, dominant current on the leeward side (Figure 10b). The asymmetry of the dunes and their geometry make it possible to deduce the direction of dune propagation, the interaction of the coastal currents and wave effects (with wave energy and patterns shown in white in Figure 10a,b). These intersecting currents lead to local sand accumulations that gradually build up above the water level. The white arrows reveal the progressive propagation and concatenation of the sand. The sinusoidal pattern observed in the coastal

geography suggests the interplay of two distinct coastal currents. One current originates from the northeast (NE), while the other comes from the northwest (NW).

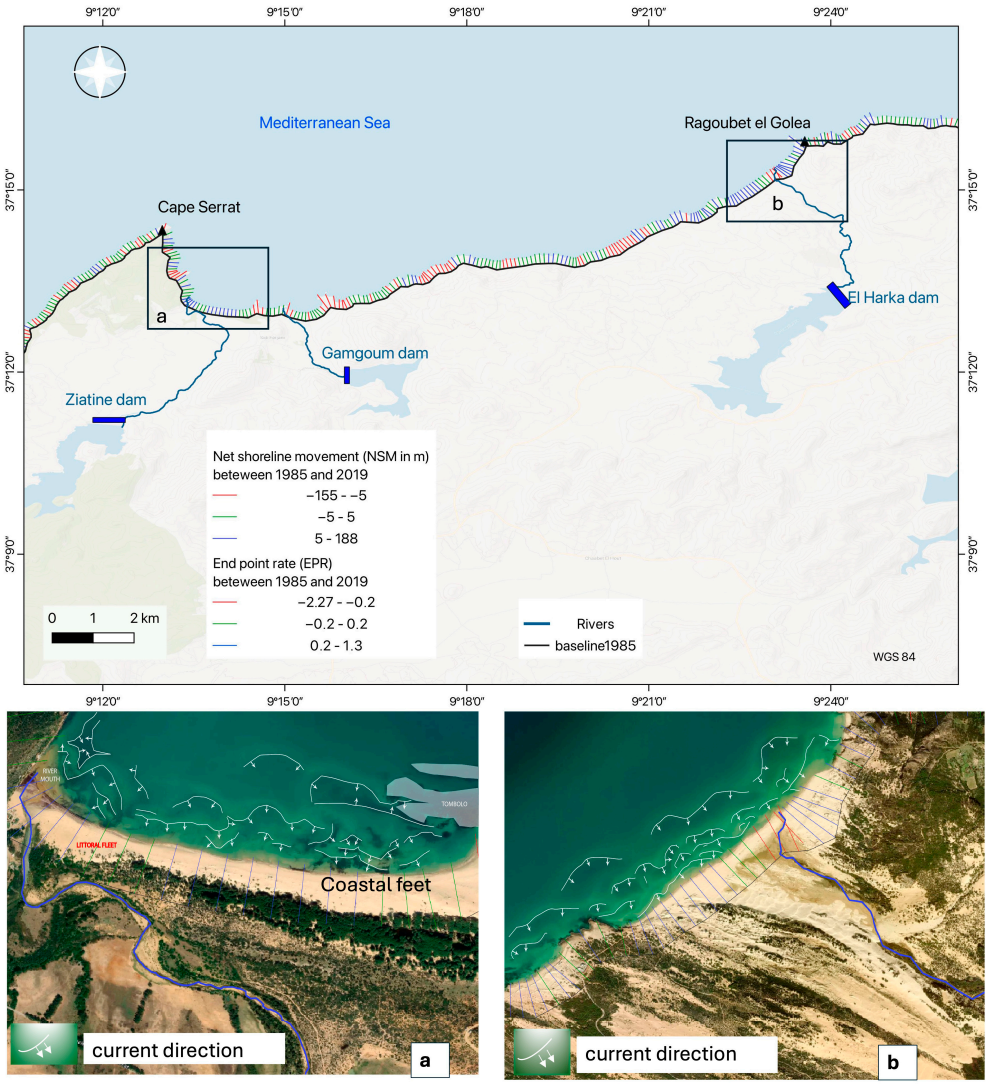

Figure 10. Examples of two dune systems in the study area: (**a**) the long dunes form caused by the interaction of multiple coastal currents or wind directions; (**b**) the short dunes form under the influence of a single, dominant current and wind direction. The white line in the sea (**a**,**b**) represents the coastal current direction.

This interaction of the currents helps explain the localized sand accumulations, which gradually build up and emerge above the water level, eventually spreading across the surface.

The construction of the dam has disrupted the natural dynamics of the river and sediment movement against the cape, leading to sediment deposition along the shore due to relatively low wave energy. This disruption significantly affects the sediment that would typically flow downstream, limiting the sand supply needed for beach maintenance. Furthermore, the reduced water flow and energy levels in coastal areas result in diminished wave action, which is essential for sediment redistribution and beach nourishment, ultimately impacting coastal accretion.

4.1.2. Dune Accumulation

As sand is transported and deposited by waves, tides, and wind, successive layers of dune are accumulated vertically over time (Figure 11a). In the submerged, near-shore zone,

the dunes are very flattened and low-lying, likely due to the influence of wave action and water currents (Figure 11b).

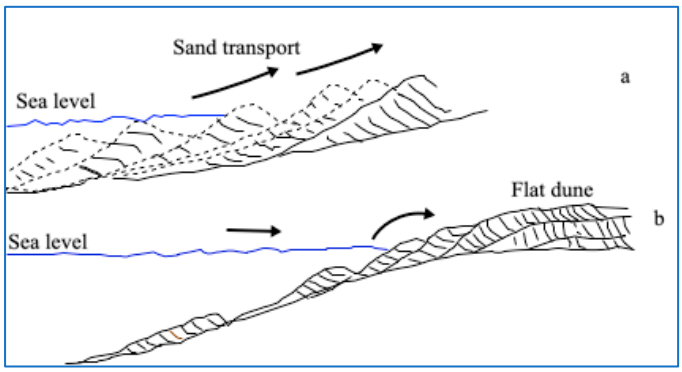

Figure 11. The retreat and removal of dunes (**a**). A series of parallel dune ridges, with the oldest dune ridges located furthest inland. (**b**) Formation and growth of flat dune deposits in zone 5 (Figure 1), characterized by semi-fixed dunes.

4.2. Wind Effects in the Cliff of Cap Serrat

The wind blows and pelts the cliff face with suspended sand particles or water droplets. This pounding leads to rock adhesion to the cliff. Wave action has a similar effect but mainly on the lower regions of the rock face, as shown in Figure 12. Strong waves act as powerful forces and bombard the cliff faces with water. The transposed sand particles, originating from strong coastline waves, act as powerful forces and bombard the cliff faces with water. This high pressure loosens the sand particles, a process known as hydraulic action. Then, the loosened particles act like sandpaper, helping to loosen other particles, like abrasive sandpaper (abrasion). These particles are abraded by currents and deposited onto the beach.

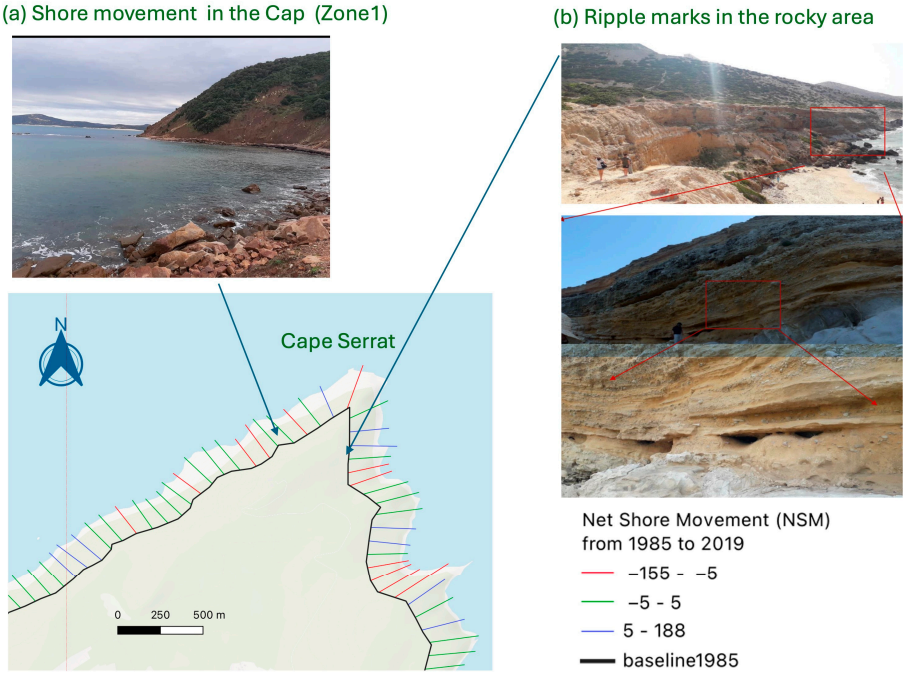

Figure 12. The coastal landscape in Cape Serrat (Figure 1, zone 1) (**a**), showing the reshaping of the rocky shoreline from 1994 to 2019. Sedimentary rock layers with visible ripple marks, highlighting geomorphological features caused by weathering and erosion in the cliff, and the abrasion phenomena in the cliff (**b**).

4.3. Waves Erosion and Deposition

Longshore drift is identified by the movement of waves along the shoreline and the transport of sediments parallel to the coast, leading to the deposition of these materials in offshore areas, creating sand dunes (Figure 13a). However, storm events or periods of high wave energy undermine the base of dunes, leading to slumping, scarping, and the formation of steep dune faces or micro cliffs (Figure 13b).

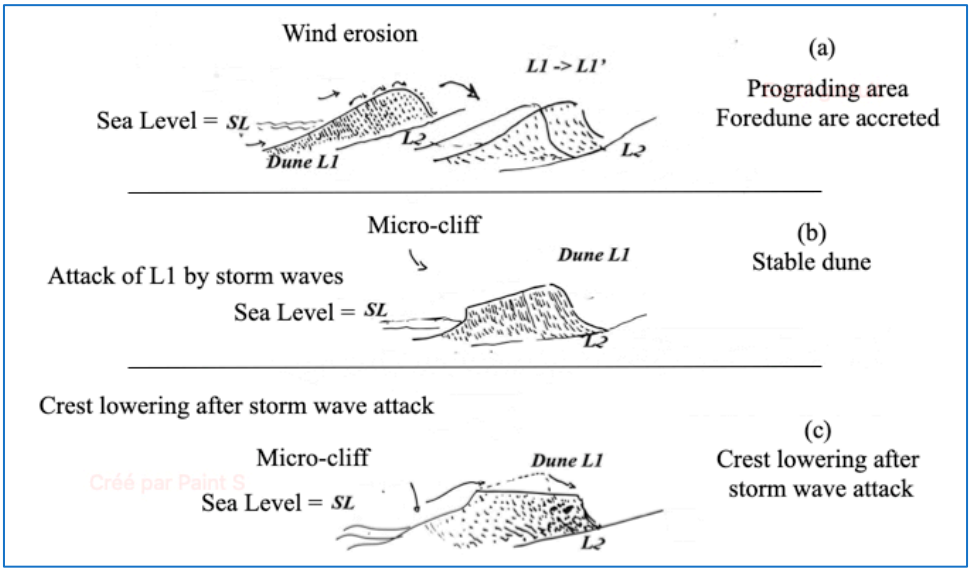

Figure 13. The dynamics of coastal erosion and dune dynamics processes, particularly in relation to waves action, dune formations, and stability. (**a**) shows the coastal features (dunes, inshore sand deposits); (**b**) the relationship between water level and micro-cliff formation caused by erosion; and (**c**) illustrates the effects of storm wave attacks on dunes.

Erosion caused by the movement of waves along the shoreline gradually wears away and erodes the shoreline (Figure 13a). The repeated wetting and drying, as well as the temperature changes caused by wave action, contribute to the weathering and erosion of coastal features (Figure 13c).

4.4. Uncertainties of Coastline Change Estimation

The uncertainties in shoreline position are associated with tides and wave storms, influenced by seasonal variability, whereas measurement uncertainties are linked to errors in image processing and digitizing conducted by technicians who identify and map the shoreline position for several observation years [14].

The position, the orientation, the distance between transects, and the smoothing rate were specified with different levels of precision, affecting the accuracy of the results obtained. However, DSAS provides an estimation of uncertainty in each transect, allowing results to be weighted based on their reliability. The distance between transects determines the spatial resolution of the calculations. A shorter distance between transects will provide a greater number of data points, which can better capture the spatial variability of the coastline.

Although the availability of a long-term time series of Landsat data between 1985 and 2019 is valuable, the spatial resolution (30 m) poses a limitation for coastline extraction. Additionally, the extracted coastlines can be corrected using the Digital Elevation Model (DEM) and/or by using in situ measurements of tides, which enhance the accuracy of shorelines monitoring [9,44].

5. Conclusions and Perspectives

This study leveraged time-series Landsat satellite imagery and geospatial analysis techniques, including the Digital Shoreline Analysis System (DSAS), to comprehensively investigate the shoreline morpho-dynamics and coastal evolution in the northern Tunisian region from 1985 to 2019.

The multitemporal remote sensing analysis revealed significant changes in the shoreline geometry and location, including the transgression of coastal dunes. The quantitative assessment using the DSAS approach showed that approximately 65% of the coastal shoreline is undergoing steady erosion near the tombolo areas. In contrast, the highest accretion rates were detected near the river mouths impacted by dam construction.

The findings also highlighted distinct seasonal variations, with maximum erosion occurring during the winter months and accretion being predominant in the spring season. These dynamic shoreline changes were attributed to a combination of natural processes, such as wave/tide action, wind transport, pedogenesis, and deposition, as well as anthropogenic influences, including coastal development, reforestation, and the installation of major dams.

The monitoring of dune evolution using high-resolution Google Earth imagery further complemented the understanding of the complex morphosedimentary processes shaping the northern Tunisian coastline.

The robust methodology employed in this study, integrating multi-temporal remote sensing data with advanced geospatial analysis techniques, has demonstrated the potential to provide a convenient and cost-effective means for maintaining and updating coastal databases. Furthermore, the comprehensive dataset generated could be leveraged to develop and illustrate future sea-level rise impact scenarios, thereby informing effective coastal management and adaptation strategies for this ecologically significant region.

Researchers are exploring the use of higher-resolution satellite or aerial imagery to further refine the spatial and temporal accuracy of the shoreline change analysis. Additionally, comprehensive monitoring and analysis of the coastal environment, considering both long-term and seasonal variations, would contribute to a deeper understanding of the complex interactions between sedimentological changes and the underlying anthropic and environmental drivers. Moreover, this study could shed light on the condition of the southern Mediterranean coastline prior to a tectonic event (such as volcano eruption), encouraging research on the secondary effects that the eruption may have on sea level rise.

Supplementary Materials: The following supporting information can be downloaded at: https://www.mdpi.com/article/10.3390/rs16203895/s1, Supplementary File S1: Data caracteristics.

Author Contributions: Conceptualization, Z.K., E.A., B.D. and M.O.; methodology, Z.K., E.A., B.D. and M.O.; software, Z.K. and E.A.; validation Z.K., B.D. and M.O.; formal analysis, Z.K., E.A., B.D. and M.O.; investigation: Z.K., E.A., B.D. and M.O.; resources, Z.K., E.A., B.D. and M.O.; data curation, Z.K., E.A. and B.D.; writing—original draft preparation, Z.K.; writing—review and editing, E.A. and B.D.; visualization, Z.K., E.A. and B.D.; supervision, Z.K. and B.D.; project administration, Z.K. and B.D. All authors have read and agreed to the published version of the manuscript.

Funding: This research received no external funding.

Data Availability Statement: The remote sensing imagery at https://www.usgs.gov/landsat-missions/landsat-data-access/ (accessed on May 2019) and the developed Earth Engine code and coastline data are available on demand.

Acknowledgments: This research was conducted under the GREEN-TEAM (InteGRatEd Management of Natural Resources: Remote Sensing, Spatial Analysis and Modeling). The authors thank the lab members for their contributions and they have consented to the acknowledgement.

Conflicts of Interest: The authors declare no conflicts of interest. The funders had no role in the design of the study; in the collection, analyses, or interpretation of data; in the writing of the manuscript; or in the decision to publish the results.

References

1. Chen, C.; Fu, J.; Zhang, S.; Zhao, X. Coastline Information Extraction Based on the Tasseled Cap Transformation of Landsat-8 OLI Images. *Estuar. Coast. Shelf Sci.* **2019**, *217*, 281–291. [CrossRef]
2. Oueslati, A.; Aroui, O.E.; Sahtout, N. Sur La Grande Vulnérabilité Du Lido Du Complexe Lagunaire de Ghar El Melh et de Ses Terres Humides (Tunisie Septentrionale): Érosion, Risque de Maritimisation et Menaces Sur Le Terroir Original Ramli. *Mediterranee* **2015**, *125*, 65–73. [CrossRef]
3. Slim, H.; Trousset, P.; Paskoff, R.; Oueslati, A.; Bonifay, M.; Lenne, J. Le Littoral de La Tunisie, Étude Géoarchéologique et Historique. *J. Mediterr. Geogr.* **2005**, *104*, 134. [CrossRef]
4. Rouvier, H.; Solignace, L.J.M. Nappe de charriage en Tunisie septentrionale: Preuves et conséquences paléogéographiques. *Tunis* **1973**, *26*, 33–47.
5. Mohamed auld Dah; Abdelhamid Khaldi; Mohamed Nejib Rejeb; Belgacem Henchi Essai de Végétalisation de Dunes Littorales: Cas Du Complexe Dunaire d'Eghirane (Mogods, Tunisie). *Sci. Et Chang. Planétaires/Sécheresse* **2005**, *16*, 255–260.
6. Dolan, R.; Hayden, B.; Heywood, J. A New Photogrammetric Method for Determining Shoreline Erosion. *Coast. Eng.* **1978**, *2*, 21–39. [CrossRef]
7. Paskoff, R.; Sanlaville, P. *Les Côtes de la Tunisie: Variations du Niveau Marin Depuis le Tyrrhénien Travail*; Collection de la Maison de l'Orient méditerranéen; Maison de l'Orient: Lyon, France, 1983; ISBN 978-2-903264-04-8.
8. Martínez, M.L.; Intralawan, A.; Vázquez, G.; Pérez-Maqueo, O.; Sutton, P.; Landgrave, R. The Coasts of Our World: Ecological, Economic and Social Importance. *Ecol. Econ.* **2007**, *63*, 254–272. [CrossRef]
9. Sun, S.; Mu, L.; Feng, R.; Chen, Y.; Han, W. Quadtree Decomposition-Based Deep Learning Method for Multiscale Coastline Extraction with High-Resolution Remote Sensing Imagery. *Sci. Remote Sens.* **2024**, *9*, 100112. [CrossRef]
10. Cooper, H.M.; Zhang, C.; Davis, S.E.; Troxler, T.G. Object-Based Correction of LiDAR DEMs Using RTK-GPS Data and Machine Learning Modeling in the Coastal Everglades. *Environ. Model. Softw.* **2019**, *112*, 179–191. [CrossRef]
11. Harley, M.D.; Turner, I.L.; Short, A.D.; Ranasinghe, R. Assessment and Integration of Conventional, RTK-GPS and Image-Derived Beach Survey Methods for Daily to Decadal Coastal Monitoring. *Coast. Eng.* **2011**, *58*, 194–205. [CrossRef]
12. Voyiadjis, G.Z.; Zhou, Y.; Abdalla, A. Creep-Induced Subsidence along Coastal Louisiana with GPS Measurements and Finite Element Modeling. *Geoenergy Sci. Eng.* **2024**, *238*, 212840. [CrossRef]
13. Madani, A. Assessment and Evaluation of Band Ratios, Brovey and HSV Techniques for Lithologic Discrimination and Mapping Using Landsat ETM+; and SPOT-5 Data. *Int. J. Geosci* **2014**, *05*, 5–11. [CrossRef]
14. Prieto-Campos, A.; Díaz-Cuevas, P.; Fernandez-Nunez, M.; Ojeda-Zújar, J. Methodology for Improving the Analysis, Interpretation, and Geo-Visualisation of Erosion Rates in Coastal Beaches—Andalusia, Southern Spain. *Geosciences* **2018**, *8*, 335. [CrossRef]
15. Dar, I.A.; Dar, M.A. Prediction of Shoreline Recession Using Geospatial Technology: A Case Study of Chennai Coast, Tamil Nadu, India. *J. Coast. Res.* **2009**, *256*, 1276–1286. [CrossRef]
16. Kang, Y.; He, J.; Wang, B.; Lei, J.; Wang, Z.; Ding, X. Geomorphic Evolution of Radial Sand Ridges in the South Yellow Sea Observed from Satellites. *Remote Sens.* **2022**, *14*, 287. [CrossRef]
17. Ge, X.; Sun, X.; Liu, Z. Object-Oriented Coastline Classification and Extraction from Remote Sensing Imagery. In Proceedings of the Remote Sensing of the Environment: 18th National Symposium on Remote Sensing of China, Wuhan, China, 20–23 October 2012.
18. Husband, E.; East, H.K.; Hocking, E.P.; Guest, J. Honduran Reef Island Shoreline Change and Planform Evolution over the Last 15 Years: Implications for Reef Island Monitoring and Futures. *Remote Sens.* **2023**, *15*, 4787. [CrossRef]
19. Liu, H.; Jezek, K.C. Automated Extraction of Coastline from Satellite Imagery by Integrating Canny Edge Detection and Locally Adaptive Thresholding Methods. *Int. J. Remote Sens.* **2004**, *25*, 937–958. [CrossRef]
20. McFEETERS, S.K. The Use of the Normalized Difference Water Index (NDWI) in the Delineation of Open Water Features. *Int. J. Remote Sens.* **1996**, *17*, 1425–1432. [CrossRef]
21. Mohanty, P.C.; Shetty, S.; Mahendra, R.S.; Nayak, R.K.; Sharma, L.K.; Rama Rao, E.P. Spatio-Temporal Changes of Mangrove Cover and Its Impact on Bio-Carbon Flux along the West Bengal Coast, Northeast Coast of India. *Eur. J. Remote Sens.* **2021**, *54*, 525–537. [CrossRef]
22. Nazeer, M.; Waqas, M.; Shahzad, M.I.; Zia, I.; Wu, W. Coastline Vulnerability Assessment through Landsat and Cubesats in a Coastal Mega City. *Remote Sens.* **2020**, *12*, 749. [CrossRef]
23. Pasquarella, V.J.; Holden, C.E.; Kaufman, L.; Woodcock, C.E. From Imagery to Ecology: Leveraging Time Series of All Available Landsat Observations to Map and Monitor Ecosystem State and Dynamics. *Remote Sens. Ecol. Conserv.* **2016**, *2*, 152–170. [CrossRef]
24. Pradhan, B.; Rizeei, H.; Abdulle, A. Quantitative Assessment for Detection and Monitoring of Coastline Dynamics with Temporal RADARSAT Images. *Remote Sens.* **2018**, *10*, 1705. [CrossRef]
25. Scardino, G.; Mancino, S.; Romano, G.; Patella, D.; Scicchitano, G. An Integrated Approach between Multispectral Satellite Images and Geophysical and Morpho-Topographic Surveys for the Detection of Water Stress Associated with Coastal Dune Erosion. *Remote Sens.* **2023**, *15*, 4415. [CrossRef]
26. Castro, I.J.; Dias, J.M.; Lopes, C.L. Assessing Shoreline Changes in Fringing Salt Marshes from Satellite Remote Sensing Data. *Remote Sens.* **2023**, *15*, 4475. [CrossRef]

27. Fabris, M.; Balin, M.; Monego, M. High-Resolution Real-Time Coastline Detection Using GNSS RTK, Optical, and Thermal SfM Photogrammetric Data in the Po River Delta, Italy. *Remote Sens.* **2023**, *15*, 5354. [CrossRef]
28. Conlin, M.P.; Adams, P.N.; Palmsten, M.L. On the Potential for Remote Observations of Coastal Morphodynamics from Surf-Cameras. *Remote Sens.* **2022**, *14*, 1706. [CrossRef]
29. Wang, J.; Wang, L.; Feng, S.; Peng, B.; Huang, L.; Fatholahi, S.N.; Tang, L.; Li, J. An Overview of Shoreline Mapping by Using Airborne LiDAR. *Remote Sens.* **2023**, *15*, 253. [CrossRef]
30. Shlien, S.; Smith, A. A Rapid Method to Generate Spectral Theme Classification of LANDSAT Imagery. *Remote Sens. Environ.* **1975**, *4*, 67–77. [CrossRef]
31. Ciecholewski, M. Review of Segmentation Methods for Coastline Detection in SAR Images. *Arch. Comput. Methods Eng.* **2024**, *31*, 839–869. [CrossRef]
32. Yan, J.; Wang, M.; Su, F.; Wang, T.; Xiao, R. Construction of Knowledge Rule Sets for the Classification of Land Cover Information for the Coastal Zone of Peninsular Malaysia. *Eur. J. Remote Sens.* **2020**, *53*, 293–308. [CrossRef]
33. Kassouk, Z.; Thouret, J.-C.; Gupta, A.; Solikhin, A.; Liew, S.C. Object-Oriented Classification of a High-Spatial Resolution SPOT5 Image for Mapping Geology and Landforms of Active Volcanoes: Semeru Case Study, Indonesia. *Geomorphology* **2014**, *221*, 18–33. [CrossRef]
34. Hu, Q.; Wu, W.; Xia, T.; Yu, Q.; Yang, P.; Li, Z.; Song, Q. Exploring the Use of Google Earth Imagery and Object-Based Methods in Land Use/Cover Mapping. *Remote Sens.* **2013**, *5*, 6026–6042. [CrossRef]
35. Rajawat, A.S.; Chauhan, H.B.; Ratheesh, R.; Rhode, S.; Bhanderi, R.J.; Mahapatra, M.; Kumar, M.; Yadav, R.; Abraham, S.P.; Singh, S.S.; et al. Assessment of Coastal Erosion along Indian Coast on 1: 25,000 Scaleusing Satellite Data. *Int. Arch. Photogramm. Remote Sens. Spat. Inf. Sci.* **2014**, *XL–8*, 119–125. [CrossRef]
36. Zhou, X.; Wang, J.; Zheng, F.; Wang, H.; Yang, H. An Overview of Coastline Extraction from Remote Sensing Data. *Remote Sens.* **2023**, *15*, 4865. [CrossRef]
37. Daud, S.; Milow, P.; Zakaria, R.M. Analysis of Shoreline Change Trends and Adaptation of Selangor Coastline, Using Landsat Satellite Data. *J. Indian Soc. Remote Sens.* **2021**, *49*, 1869–1878. [CrossRef]
38. Surf Forecast in Cap Serrat Including Swell, Period, Wind and Tides in Cap Serrat for the Next Few Days. Available online: https://tides4fishing.com/tn/tunisia/cap-serrat/forecast/surf (accessed on 21 July 2019).
39. Luijendijk, A.; Hagenaars, G.; Ranasinghe, R.; Baart, F.; Donchyts, G.; Aarninkhof, S. The State of the World's Beaches. *Sci. Rep.* **2018**, *8*, 6641. [CrossRef]
40. Sayre, R.; Noble, S.; Hamann, S.; Smith, R.; Wright, D.; Breyer, S.; Butler, K.; Van Graafeiland, K.; Frye, C.; Karagulle, D.; et al. A New 30 Meter Resolution Global Shoreline Vector and Associated Global Islands Database for the Development of Standardized Ecological Coastal Units. *J. Oper. Oceanogr.* **2019**, *12*, S47–S56. [CrossRef]
41. Morhange, C. H. Slim, P, Trousset, R, Paskoff et A. Oueslati, et al., Le littoral de la Tunisie, étude géoarchéologique ethistorique. *Mediterranee* **2005**, *134*, 308.
42. Surf Forecast in Cap Serrat Including Swell, Period, Wind and Tides in Cap Serrat for the Next Few Days. Available online: https://tides4fishing.com/ (accessed on 9 March 2019).
43. Potić, I. Simple ETM+ Gap Fill Techniques Review. *Environment* **2015**, *3*, 31–37.
44. Potere, D. Horizontal Positional Accuracy of Google Earth's High-Resolution Imagery Archive. *Sensors* **2008**, *8*, 7973–7981. [CrossRef]
45. Goodchild, M.F. The Use Cases of Digital Earth. *Int. J. Digit. Earth* **2008**, *1*, 31–42. [CrossRef]
46. Yıldırım, C. Geomorphology of Horseshoe Island, Marguerite Bay, Antarctica. *J. Maps* **2020**, *16*, 56–67. [CrossRef]
47. Zhao, Y.; Diao, C.; Augspurger, C.K.; Yang, Z. Monitoring Spring Leaf Phenology of Individual Trees in a Temperate Forest Fragment with Multi-Scale Satellite Time Series. *Remote Sens. Environ.* **2023**, *297*, 113790. [CrossRef]
48. Kaut, R.J.; Thomas, G.S. The Tasselled Cap—A Graphic Description of the Spectral-Temporal Development of Agricultural Crops as Seen by LANDSAT. In Proceedings of the Symposium on Machine Processing of Remotely Sensed Data, Purdue, Indiana, 21–23 June 1977.
49. Thieler, E.R.; Himmelstoss, E.A.; Zichichi, J.L.; Ergul, A. *The Digital Shoreline Analysis System (DSAS) Version 4.0-an ArcGIS Extension for Calculating Shoreline Change*; US Geological Survey: Asheville, NC, USA, 2009.
50. Thinh, N.A.; Hens, L. A Digital Shoreline Analysis System (DSAS) Applied on Mangrove Shoreline Changes along the Giao Thuy Coastal Area (Nam Dinh, Vietnam) during 2005–2014. *J. Sci. Earth* **2017**, *39*, 87–96. [CrossRef]